REVIEW PAPER

Primary estimation of metal hydride electrode performance

Ivan Saldan

Abstract A review on general electrochemical processes for metal hydride (MH) electrodes has been done. Fundamental MH electrode characteristics responsible for $(-)MH_x/M|6M\ KOH|xNi(OH)_2/xNiOOH(+)$ accumulator performance have been discussed in detail. Some examples of hydrogen storage alloys with permanent interest as MH electrodes have been presented.

Keywords Equilibrium potential of MH electrode · Electrocatalytic activity · Discharge capacity · Cycle stability · Hydrogen storage alloy

Introduction

Considering advantages of hydrogen energy with respect to energy sources based on fossil fuels, the alkaline nickel–metal hydride (Ni–MH) batteries find more often application today instead of well-known Ni–Cd ones. MH electrodes can be operated at high current density and low temperatures and are considered less harmful for the environmental than Cd. These properties determine their application as portable batteries [1–4]. Replacing the Ni–Cd galvanic cell by the Ni–MH does not result in considerable change of discharge potential (1.25–1.3 V). Furthermore,

due to specific mechanism of hydrogen transfer in solid for MH electrodes, the Ni–MH batteries usually are featured with higher reliability and smaller size. For example, the theoretical discharge capacity of $LaNi_5H_6$ metal hydride amounts to ~375 A·h/kg or 2,600 A·h/l, and in this material, 1 g of hydrogen can supply ~27-A·h current. Of course, this may vary for particular hydrogen-absorbing alloys for which a different value of discharge capacity can be achieved. Another aspect of hydrogen-absorbing alloys is their commercial price. Nevertheless, the theoretical discharge capacities of manufacturing MH electrodes is two to three times higher in comparison to Cd ones. Specific energy of Ni–MH batteries amounts up to 55–75 W/kg or 180–210 W/l, which is 20–30% higher by mass and 50–100% by volume density with respect to Ni–Cd. At the moment, the working life of MH electrodes is ~1,000 charge–discharge cycles depending on the electrode characteristics and manufacturing methods, which is considerably less than for commercial Ni–Cd accumulators that are characterized by cycle life of up to 2,000 cycles and more.

In order to overcome this disadvantage of Ni–MH batteries, the main attention should be focused on the study of MH electrode with respect to processes at electrode surface of hydrogen-absorbing alloys and the technology development of electrode material preparation. Moreover, the highest emphasis must be laid up as following: chemical stability of all components of MH electrode in alkaline solution, their physical and mechanical reliability, overvoltage under desirable current density, charge transfer mechanism, and behavior of atomic hydrogen transfer in solid bulk [5].

Since the 1970s, we have got a lot of characteristics of metal hydrides which were synthesized mostly by hydrogen gaseous method. At the same time, there is not so much information about their application as effective MH electrodes in detail. It
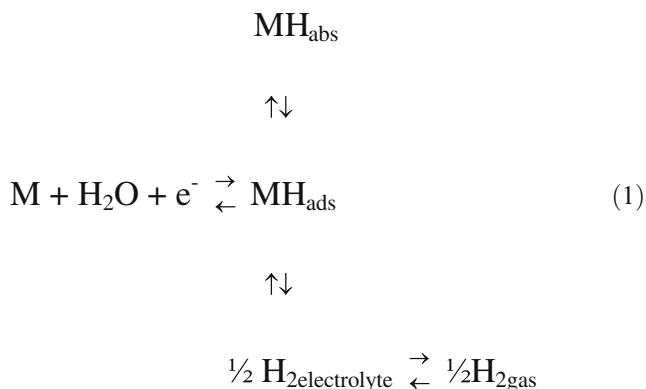
I. Saldan (✉)
Lviv Polytechnic National University,
MSL, 1 Kotliarevsky St,
79013 Lviv, Ukraine
e-mail: ivan_saldan@yahoo.com

I. Saldan
Florida International University,
CeSMEC, 11200 SW 8th St,
Miami, FL 33199, USA

seems not to be easy to combine the properties of hydrogen-absorbing alloys together with electrolyte [6–8]. Owing to the existence of various influences (with different force and direction) under MH electrode performance, we should consider electrochemical hydrogenation/dehydrogenation as a total process of miscellaneous impacts. Thus, we can improve electrode characteristics and, consequently, the entire Ni–MH battery.

Electrochemical processes on the surface of MH electrode

Under cathode polarization of MH electrode in electrolyte, gaseous hydrogen evolution takes place together with accumulation of dissolved hydrogen into the bulk of alloy/metal. The electrochemical hydrogenation is a multi-stage process and for simplicity can be written only by four steps:

$$MH_{abs}$$

$$\uparrow\downarrow$$

$$M + H_2O + e^- \underset{\leftarrow}{\rightarrow} MH_{ads} \tag{1}$$

$$\uparrow\downarrow$$

$$\tfrac{1}{2} H_{2electrolyte} \underset{\leftarrow}{\rightarrow} \tfrac{1}{2}H_{2gas}$$

Charge transfer reaction, which occurs directly on the MH electrode/electrolyte surface, can be introduced by Max Volmer reaction:

$$(H_2O)_{surface} + e^- \underset{\leftarrow}{\rightarrow} H_{ads} + (OH^-)_{surface} \tag{2}$$

As a result, atomic hydrogen chemically adsorbs on the surface. Then, hydrogen atoms can be transferred by diffusion into the bulk of the solid. At the same time, recombination of two chemically adsorbed hydrogen atoms takes place on the surface of MH electrode. This hydrogen recombination leads to dissolution of molecular hydrogen in electrolyte $H_{2electrolyte}$. Finally, the equilibrium between $H_{2electrolyte}$ and gaseous hydrogen, H_{2gas}, will be achieved. The hydrogen gas formation can be written by Julius Tafel reaction:

$$2H_{ads} \underset{\leftarrow}{\rightarrow} H_{2\,gas} \tag{3}$$

Consequently, charge efficiency for MH electrode is obtained as speed ratio of hydrogen diffusion into the bulk of solid to the hydrogen desorption into the bulk of

electrolyte. The chemical potential for surface hydrogen is characterized by degree of surface occupation by adsorbed hydrogen atoms. The hydrogen chemical potential of the bulk is determined by total portion of occupied absorbed centers. Therefore, the difference between chemical potential of hydrogen on the surface and in the solid bulk is the driving force of alloy/metal hydrogenation, and in the case of MH electrode, it should be the electrochemical hydrogenation motive.

Equilibrium potential of MH electrode

Equilibrium potential of MH electrode ($\phi_{MH,eq}$), the Gibbs free energy change (ΔG_{MH}), equilibrium hydrogen pressure (P_{eq}), and chemical potential (μ_i) correlate each other as follows:

$$\Delta G_{MH} = \sum v_i\mu_i = RT\ln\left(P_{eq}/P^o\right) = nF\varphi_{MH,eq} \tag{4}$$

where R is the gas constant; T is the temperature; P^o is the standard pressure (1 bar); n is the amount of electron, which takes part at hydrogenation; and F is the Faraday constant.

In a recent work [9], a mathematical model which describes miscellaneous physical–chemical processes, which appear on the surface of MH electrode, was presented. The characteristic of proper chemical flows has been done using drawing of electrochemical hydrogenation. The model of lattice gas was used to describe the thermodynamics for hydrogen insertion. For simplicity, the model of average field was used that assumes far interaction between hydrogen atoms. The equilibrium potential of MH electrode measured in that way gives us a very good compliance with experimental data, obtained by hydrogen pressure content (PC) isotherms. Thus, the system of three equations for $\varphi_{MH,eq}$ can be shown in the following way:

$$\varphi_{MH}^o = \begin{cases} \varphi_1^o + (T - T_{rel})\dfrac{\Delta S_{298}^o}{nF} + \dfrac{RT}{nF}\left(\ln\left[\dfrac{1-x}{x}\right] - U_\alpha x\right), x < x_\alpha \\ k_\varphi x + C, \; x_\alpha \le x \le x_\beta \\ \varphi_2^o + (T - T_{rel})\dfrac{\Delta S_{298}^o}{nF} + \dfrac{RT}{nF}\left(\ln\left[\dfrac{1-x}{x}\right] - U_\beta x\right), x < x_\beta \end{cases}$$
$$\tag{5}$$

where φ^o is standard electrode potential for i-phase; T_{rel} is the relative temperature (298 K); x is the molar content of hydrogen in MH electrode; and k_φ i C are the coefficients, which are dependent on the interaction energy and standard potential for every phase.

When hydrogenation process reaches the equilibrium, partial hydrogen pressure in metal hydride is P_{eq}. It is known that the equilibrium potential of MH electrode should

correlate with equilibrium hydrogen pressure by Nernst equation, and the values of this potential with respect to reference electrode (e.g., HgO/Hg) can be determined as follows [5]:

$$\varphi_{MH,eq}\left(\text{with regards to } \varphi_{HgO/Hg}\right)$$
$$= \left(\varphi_H^o - \varphi_{HgO/Hg}^o\right) + RT/2F \ln[a(H_2O)/a(H_2)] =$$
$$= \left(\varphi_H^o - \varphi_{HgO/Hg}^o\right) + RT/2F \ln\left[a(H_2O)/\gamma(H_2)P_{eq}\right],$$
(6)

where $a(H_2O)$ and $a(H_2)$ are the activity for water and hydrogen, respectively and $\gamma(H_2)$ is the coefficient of fugacity for gaseous hydrogen. If we know the values of $a(H_2)$ and $\gamma(H_2)$ in electrolyte (which is given as a function of temperature and concentration of KOH solution), the last equation can be simplified in the following way:

$$\varphi_{MH,eq}\left(\text{with regards to } \varphi_{HgO/Hg}\right)$$
$$= -0.9324 - 0.0291 \log P_{eq}$$
(7)

The last equation shows us the dependence between $\varphi_{MH,eq}$ and P_{eq} in 6 M KOH solution at 293 K and standard pressure ($P^o=1$ bar). Thus, in order to obtain Eq. 7, we must have all values for the standard potentials, water activity, and coefficient of fugacity that might be difficult to get [10].

Therefore, another method which uses thermodynamics of Ni–MH accumulator was proposed [11]. In general, exothermic reaction of hydrogen absorption can be written as follows:

$$M + x/2\ H_2 \underset{\leftarrow}{\rightarrow} MH_x + \Delta H$$
(8)

For chemical $(-)MH_x/M|6M\ KOH|xNi(OH)_2/xNiOOH(+)$ cell, the total electrochemical reaction can be drawn as:

$$MH_x + xNiOOH \underset{\leftarrow}{\rightarrow} M + xNi(OH)_2,$$
(9)
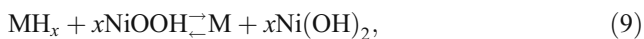
and the Gibbs free energy change should be as follows:

$$\Delta G_{cell}^0 = x\left(\Delta G_{Ni(OH)2}^0 - \Delta G_{NiOOH}^0\right)$$
$$- \left(\Delta G_{MHx}^0 - \Delta G_M^0\right)$$
(10)

The voltage on the clams of this chemical cell must be as:

$$\varphi_{cell}^o = \varphi_{(+)}^o - \varphi_{(-)}^o = \Delta G_{cell}^0/xF,$$
(11)

where $\varphi_{(+)}^0$ and $\varphi_{(-)}^0$ are the positive and negative potential with respect to HgO/Hg reference electrode. If we bear in mind hydrogen as ideal gas, the van't Hoff equation would be correct for hydrogen absorption reaction, and the Gibbs

free energy change for hydrogenation at MH electrode can be written as follows:

$$\Delta G^0 = \Delta G_{MHx}^0 - \Delta G_M^0$$
(12)

From van't Hoff and Eqs. 10–12, the dependency of $\varphi_{(-)}^0$ on P_{eq} ($P^0=1$ bar) can be derived:

$$\varphi_{(-)}^0 = \varphi_{(+)}^0 + \left(\Delta G_{Ni(OH)2}^0 - \Delta G_{NiOOH}^0\right)/F - RT$$
$$\times \ln(P_{H2})/xF$$
(13)

If we take values $\varphi_{(+)}^0 = 0.49$ V (with regards to $\varphi_{HgO/Hg}$); $\Delta G_{Ni(OH)2}^0 = -459.07$ kJ/mol; $\Delta G_{NiOOH}^0 = -321.7$ kJ/mol; $R=8.314$ J/K·mol; $T=298.15$ K; $F=96487$ A·s/mol, the last equation can be simplified significantly to the following expression:

$$\varphi_{(-)}^0\left(\text{with regards to } \varphi_{HgO/Hg}\right)$$
$$= -0.9337 - \left(0.0592 \log P_{eq}\right)/x.$$
(14)

If for electrochemical reaction 9 $x=2$, Eq. 14 will be identical to 7. However, there is variance on the correct value of x in many studies of MH electrodes. Different quantities of hydrogen atoms x absorbed by alloy/metal lead to the idea that the potential of MH electrode should be changed depending on hydrogen storage material properties. In other words, $\varphi_{(-)}^0$ depends on the type of hydrogen absorber. Equation 14 should give the same result as 7 since in the last, the number of electrons, which take part in electrochemical reaction 10 and at the same time effect on equilibrium potential of MH electrode in Nernst equation, is determined. Relationship 7 or 14 shows us that when hydrogen pressure changes by one order, the potential of MH electrode should be changed on 0.0291 V; or when $\varphi_{MH,eq}$ value (with regards to $\varphi_{HgO/Hg}$) increases from -0.93 to -0.64 V, the P_{eq} value should be decreased from 1 to 10^{-10} bar. That method is quite convenient to draw PC isotherms in the 10^2-to 10^{-8}-bar pressure range using small samples (some milligrams in weight). Hydrogen pressure monitoring is one of the most important requirements for MH electrodes. In fact, if P_{eq} value is more than the hydrogen pressure in a chemical cell, the charge efficiency should be decreased, and if less, it should be difficult to activate MH electrode. Therefore, the equilibrium hydrogen pressure accepted to Ni–MH accumulators should be something less than 1 bar at 333 K temperature.
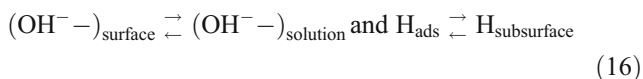
Electrocatalytic activity of MH electrode

Whole electrochemical hydrogenation is quite difficult since it is a multi-stage process; moreover, parallel chemical reactions can be possible in the electrolyte solution, for example corrosion. For a detailed review on
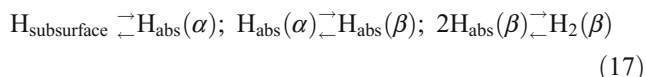
the mechanism of electrochemical hydrogenation, the most important reactions can be taken into account. Firstly, the diffusion of reactive particles from the bulk of alkaline solution to the electrode/electrolyte interface can be written as follows [5]:

$$(H_2O)_{solution} \overset{\rightarrow}{\underset{\leftarrow}{}} (H_2O)_{surface} \qquad (15)$$

Then, charge transfer reaction which was mentioned above as Max Volmer reaction (2) takes place. The motion of hydroxyl ions into the electrolyte solution and diffusion adsorbed hydrogen atoms in subsurface layer of atomic atoms [5]:

$$(OH^-)_{surface} \overset{\rightarrow}{\underset{\leftarrow}{}} (OH^-)_{solution} \text{ and } H_{ads} \overset{\rightarrow}{\underset{\leftarrow}{}} H_{subsurface} \qquad (16)$$

The next step should be the transfer of atomic hydrogen into the bulk of hydrogen storage alloys/metal. So that hydrogen diffusion can be written in three steps as minimum, which include dissolution hydrogen atoms in α-phase (hydrogen solid solution at small hydrogen concentration), $\alpha \rightarrow \beta$ phase transfer, and dissolution of molecular hydrogen in β-phase (hydrogen solid solution at bigger hydrogen concentration):

$$H_{subsurface} \overset{\rightarrow}{\underset{\leftarrow}{}} H_{abs}(\alpha); \ H_{abs}(\alpha) \overset{\rightarrow}{\underset{\leftarrow}{}} H_{abs}(\beta); \ 2H_{abs}(\beta) \overset{\rightarrow}{\underset{\leftarrow}{}} H_2(\beta) \qquad (17)$$

Desorption of adsorbed hydrogen can appear by simple Julius Tafel reaction (3) and at the same time by more sophisticated Jaroslav Heyrovsky:

$$H_{ads} + (H_2O)_{surface} + e^- \overset{\rightarrow}{\underset{\leftarrow}{}} H_{2electrolyte}$$
$$+ (OH^-)_{surface} \qquad (18)$$
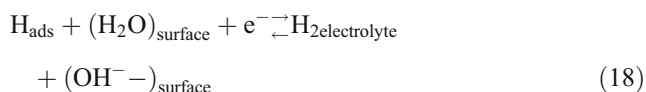
The determination of the limiting stage for whole process and the velocities of separate reactions are the actual problem for electrochemical kinetics and electrocatalysis. For example, the hydrogen evolution at MH electrode surface based on Pd can be described by the Volmer–Tafel mechanism very well. Total overvoltage for the process equals the overvoltage sum of separated reactions (2 and 3), which can be defined by $(\eta \times i)$ curves of potential decreasing/increasing after turning off/on the polarizing current. Hydrogen evolution kinetics on palladium electrodes was observed taking into account some limit stages that allowed describing the experimental polarization $(\eta \times \lg i)$ curves in detail. The Volmer–Tafel mechanism was confirmed for MH electrodes based on LaNi$_5$ and Ti–Ni alloys; moreover, the exchange in current values in both stages are comparable ($\sim$0.3–3 μA/cm^2) [12]. The slope for linear $(\eta \times \lg i)$ ranges reaches $\sim$0.12 V; therefore, the velocity of the whole process at the high overvoltage values

should be determined by charge transfer stage. Exchange current ($i_{ch,exp}$), which is obtained by that relationship extrapolation at $\eta = 0$, differs from i_{ch} value, which is calculated using the relation [5]:

$$1/i_{ch} = 1/i_{ch,Volmer} + 1/i_{ch,Tafel} \qquad (19)$$

At the same time, it was found that all $i_{ch,exp}$ values for LaNi$_5$ and Ti–Ni alloys even for Ni were very close. This fact tells us that electrocatalytic activity for these alloys must be determined by nickel, and the synergetic effect for consistent presence La with Ni or Ti with Ni appears very weakly. By the way, evidently, the $i_{ch,Volmer}/i_{ch,Tafel}$ ratio for certain alloy reveals the mixing origination of the limit stage. At cathode polarization, the $(\eta \times P_{H2})$ relationship is determined by the mechanism of hydrogen evolution reaction and correlation of exchange current for different stages. In the case of Volmer–Tafel mechanism, the ratio of hydrogen pressure at polarization ($P_{H2,pol}$) to hydrogen pressure at equilibrium potential (P_{eq}) deals with portion overvoltage for Tafel stage [13]:

$$\eta_{Tafel} = RT/2F \ln(P_{H2,pol}/P_{eq}) \qquad (20)$$

Therefore, the electrocatalytic activity of MH electrode for hydrogen evolution reaction can be estimated by the well-known Tafel equation:

$$\eta = \varphi - \varphi_{MH,eq} = a - b \log i, \qquad (21)$$

where φ is the potential of MH electrode when the hydrogen evolution reaction starts; $a = 2.3RT/\varepsilon F \log i_{ch}$; $b = 2.3RT/\varepsilon F$; and ε is the symmetrical factor. For charge transfer reaction, the exchange current density increases with increasing of electrocatalytic activity. However, in practice, we can get only the ratio of current density to mass or surface area unit. It means that exchange current density becomes the criterion of surface activity and the last includes two factors—reaction effective area and catalytic activity.

One of the best ways to reach high kinetics for electrochemical hydrogenation is the improving of internal properties of hydrogen storage alloy/metal. Therefore, it is very important to determine the activity of every component with respect to hydrogen mobility and hydrogen oxidation. The special electrocatalytic additions, which is predicted by theory of IMC lattice structure for dominant alloy phase (Brawer–Engel theory), are chosen to ameliorate the catalytic activity of hydrogen storage alloy/metal in alkali solution in practice [13]. These electrocatalytic additives constitute IMC with nickel or cobalt (Ni$_3$Mn, NiMn, Ni$_3$Fe, Ni$_3$Cr, Ni$_3$V, Ni$_3$Mo, Ni$_4$Mo, Ni$_3$W, Co$_3$Mo, Co$_3$W, and others) and are characterized by more fragmentation and higher melting point than the parent phase. The charge transfer reaction on the surface of the MH electrode with electrocatalytic addition is shown schematically in Fig. 1.
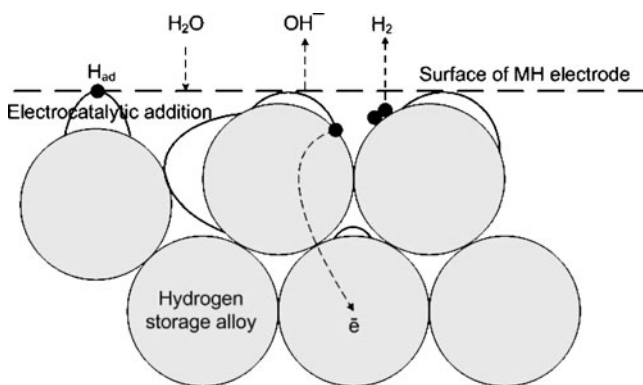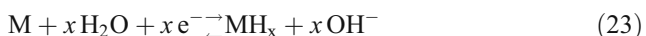
Fig. 1 Charge transfer reaction on the surface of MH electrode with electrocatalytic addition

Since phase grain boundaries become the points for active hydrogen penetration into the bulk of main IMC phase, hydrogen sorption on the surface of hydrogen storage alloy/metal can be improved owing to these electrocatalytic additives. Experimental confirmation of this hypothesis was done by P.H.L. Notten who showed that stoichiometry change of surface nickel layer by secondary phase formation (electrocatalytic additions) directly in the phase grain boundaries results in improvement of MH electrode performance [5].

Thus, for better performance of MH electrode, we can use miscellaneous electrocatalytic additives and also apply different methods to increase the electrode active surface [14]. The last can be amplified by hetero-phase factor with the use of very fine powders by special structure formation with different size powders.

Principle MH electrode characteristics

Ni–MH accumulator consists of two electrodes which are immersed in 6 M KOH aqua solution that is a medium for ion conductivity between the electrodes. The last are electrically isolated from each other by a special separator. Since MH electrode has higher capacity with respect to Ni(OH)$_2$ electrode, the gas recombination reaction is facilitated in hermetic Ni–MH cells. Under the charging, two-valence nickel is oxidizing to three-valence condition and water, which is reducing to hydrogen atoms on the surface of MH electrode and at the same time H atoms are absorbing into IMC bulk:
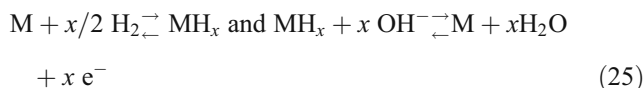
$$x\,Ni(OH)_2 + x\,OH^- \underset{\leftarrow}{\overset{\rightarrow}{-}} x\,NiOOH + x\,H_2O + x\,e^- \qquad (22)$$

$$M + x\,H_2O + x\,e^- \underset{\leftarrow}{\overset{\rightarrow}{-}} MH_x + x\,OH^- \qquad (23)$$

OH$^-$ ions and molecules of water move from one electrode to another very easily. Thus, any loss of electrolyte should be at charge–discharge processes.

Under overdischarging, hydrogen evolution starts on the Ni(OH)$_2$ electrode:

$$x/2\,H_2O + x\,e^- \underset{\leftarrow}{\overset{\rightarrow}{}} 1/4\,H_2 + x/2\,OH^- \qquad (24)$$
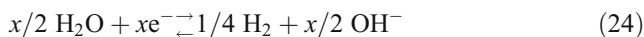
and then molecular hydrogen can diffuse through the separator to the MH electrode surface where dissociation into hydrogen atoms takes place, and straightaway, charge transfer reaction starts again:

$$M + x/2\,H_2 \underset{\leftarrow}{\overset{\rightarrow}{}} MH_x \text{ and } MH_x + x\,OH^- \underset{\leftarrow}{\overset{\rightarrow}{}} M + x\,H_2O$$
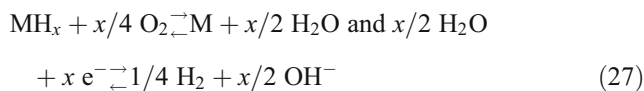$$+ x\,e^- \qquad (25)$$

Of course, rate of the first (25) reaction is not high and depends on electrode structure and also catalytic activity of the MH electrode surface where three phases are in contact with each other simultaneously: hydrogen gas/solid IMC/electrolyte. Overvoltage potential is the sum of overvoltage of both (25) reactions and amounts to ~0.2 V at the small discharging without pressure increasing.

In the case of overcharging, MH electrode forms metal hydride permanently until Ni(OH)$_2$ electrode starts oxygen evolution by the following reaction:

$$x\,OH^- \overset{\rightarrow}{} x/4\,O_2 + x/2\,H_2O + x\,e^- \qquad (26)$$
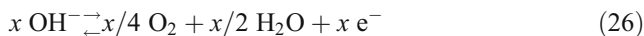
Oxygen diffuses through the separator to the MH electrode surface where it reacts, producing water that prevents pressure increasing in the hermetic cell:

$$MH_x + x/4\,O_2 \underset{\leftarrow}{\overset{\rightarrow}{}} M + x/2\,H_2O \text{ and } x/2\,H_2O$$
$$+ x\,e^- \underset{\leftarrow}{\overset{\rightarrow}{}} 1/4\,H_2 + x/2\,OH^- \qquad (27)$$

Oxygen amount which releases on Ni(OH)$_2$ electrode equal to that is recombined on the MH electrode at equilibrium conditions; thus, internal gas pressure should be constant. In order to decrease the gas diffusion through the separator, the electrolyte solution can be minimized. When hydrogen amount in metal hydride is very high, hydrogen evolution reaction on the surface of MH electrode takes place, and consequently, it results to pressure increasing in the galvanic cell.

Pressure and temperature increasing in Ni–MH cell

All molecular oxygen should be transferred to the surface of MH electrode for its full recombination. The authors of [9] derived the equation of reaction current taking into account combined kinetic/diffuse processes for oxygen recombination:

$$I_{rec} = \left(I_{rec,\,kin} \times I_{rec,\,dif}\right) / \left(I_{rec,\,kin} + I_{rec,\,dif}\right), \qquad (28)$$

where $I_{rec,kin}$ is the kinetic current and $I_{rec,dif}$ is the diffuse current which depends on electrode surface area and

average thickness of diffuse layer through which oxygen should move. Since oxygen reduction takes place at high temperatures, oxygen diffusion should be a limiting stage at oxygen recombination process. Partial oxygen pressure ($P_{O2, \text{part}}$) in Ni–MH cell can be estimated as the difference between oxygen produced on Ni(OH)$_2$ electrode and that used on MH electrode. Partial hydrogen pressure consists of thermodynamically determined equilibrium hydrogen pressure (see Eq. 4) and kinetic part of hydrogen pressure (P_{kin}), which can be determined by scheme 1 with taking into account different flows [9]:

$$P_{H2,\text{part}} = P_{\text{eq}} + P_{\text{kin}} \tag{29}$$

When any possibility of gas evolution from Ni–MH accumulator construction is predicted, the total pressure for the hermetic cell ($P_{\text{Ni–MH}}$) should be the sum of pressure for O$_2$↑ and H$_2$↑ [9]:

$$P_{\text{Ni–MH}} = P_{O2,\text{part}} + P_{H2,\text{part}} \tag{30}$$

Temperature of Ni–MH cells depends on heat flow (Q_{enter}) which is produced at their performance and can be measured by electrochemical processes of both electrodes (22 and 23) and heat dissipation into environment Q_{exit} [9]:

$$dT/dt = (Q_{\text{enter}} - Q_{\text{exit}})/C_{\text{Ni–MH}}, \tag{31}$$

where $C_{\text{Ni–MH}}$ is the heat capacity for the whole Ni–MH accumulator.

Estimation of discharge capacity for MH electrode

At electrochemical hydrogen absorption/desorption on the MH electrode (23), every H atom corresponds to one electron charge. Using Faraday's second law, the discharge capacity can be calculated theoretically as the amount of electricity which goes through the external electric circle at discharging during the time (τ):

$$C_{\text{theor}} = M \times F/q, \tag{32}$$

where M is the active substance mass; F is the Faraday constant; and q is the equivalent mass. In practice, discharge capacity always is a little less than theoretical since the reagents as usual are not used entirely. So the ratio of hydrogen evaluated at discharging to hydrogen calculated by Faraday's second law (32) very often called current yield can be written as follows:

$$L = C/C_{\text{theor}} \tag{33}$$

Experimental discharge capacity (C_{exp}) can be obtained by discharge curves (φ_{MH} (with regards to $\varphi_{\text{HgO/Hg}}$) × τ) where in galvanostatic regime continued potential change during τ is fixed. Majority of the charged MH electrodes

reach −(0.9–1.3 V, with regards to $\varphi_{\text{HgO/Hg}}$) for top limit and main portion hydrogen evolution observed at nearly −(0.9–0.7 V, with regards to $\varphi_{\text{HgO/Hg}}$). However, MH electrode testing should be stopped at incomplete discharging ≈ −(0.7 − 0.6 V) (with regards to $\varphi_{\text{HgO/Hg}}$) since irreversible reaction probability on hydrogen storage alloy/metal oxidation increases at more positive potentials. Usually, the linear range of discharge curve which corresponds to ($\alpha + \beta$) phase coexistence is taken into account (Fig. 2) [5].

Thus, at MH electrode testing in galvanostatic regime, we should accurately determine discharge time which obviously depends on the total pressure and temperature in hermetic Ni–MH cell, and consequently, C_{exp} can be measured as follows:

$$C_{\text{exp}} = i \times \tau, \tag{34}$$

where i is the applied current density. The relationship between maximum C_{exp} (or in other words complete discharge capacity (C^0)) and C_{theor} can be written as follows:

$$C^0 = C_{\text{thoer}} \times \eta. \tag{35}$$

In order to determine complete discharge capacity of MH electrode, measuring the charge/discharge curves should be carried out at equilibrium conditions, i.e., at very small charge/discharge current. Practically, after passage of certain electricity quantities, the electric circle should be cut off and the value of "open circuit potential" (equilibrium) potential must be fixed, and after that, the dependency between passed electricity quantity and the potential should be built. That method allows us to avoid some mistakes which deal with decelerated stages of hydrogen sorption, especially diffusion into the IMC bulk. The other handy method (but less accurate) to determine C^0 can be discharge capacity determination at very high (C_{high}) and very slow (C_{slow}) current (as usual $C_{\text{high}} \geq C_{\text{slow}}$). In that case, the complete discharge capacity of MH electrode can be measured as [15]:
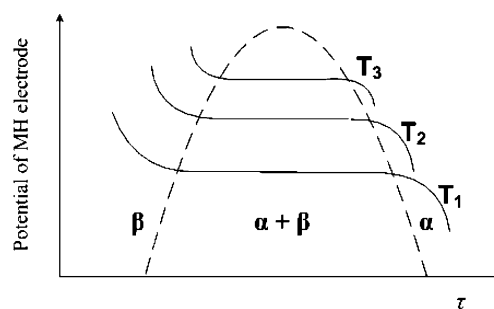
$$C^0 = C_{\text{high}} + C_{\text{slow}} \tag{36}$$

Fig. 2 Temperature dependency for discharge curves ($T_1 < T_2 < T_3$)

MH electrode stability at charge–discharge cycling

Another major characteristic of MH electrode is cycle stability (S^n) which very often determines the working life of the whole Ni–MH accumulator and can be estimated at the certain number of charge–discharge cycles (n) as follows:

$$S^n = C^n / C^0 \qquad (37)$$

Moreover, for better demonstration and convenience, the ($S^n \times n$ or $C^n/C^0 \times n$) dependency can be easily drawn (Fig. 3).

As a rule, only discharge capacity change up to 50% is taken into account. In other words, the number of cycles which corresponds to the half decay discharge capacity qualifies the working life of that Ni–MH accumulator.

High MH electrode stability at non-expendable cycling depends very much on the IMC and binding material and also the entire method of electrode preparation. Increasing cycle stability with decreasing grain size of hydrogen storage alloy/metal was confirmed experimentally. It can be explained by the appearance of a protective oxide layer on the surface of alloy particle and grain limits. In this case, the efficiency of the layer should remain unless the particles degrade to grain size. In practice, at slow cooling of alloy or annealing procedure, the ~50-μm grain size structure can be achieved, while quick quenching results in more granulate structure with ~10-μm grain size [16].

At the same time, grain disintegration to finer particles for hydrogen storage alloy/metal at charge–discharge cycling can stimulate corrosion processes. When AB_n alloy contacts with 6 M KOH aqua solution, some chemical reactions should take place on the surface of the MH electrode [16]:

$$AB_n + 3\,H_2O \underset{\leftarrow}{\rightarrow} A(OH)_3 + nB + 3H_2 \qquad (38)$$

$$2AB_n + (2n + 6)\,H_2O \underset{\leftarrow}{\rightarrow} 2A(OH)_3 + 2nBO$$
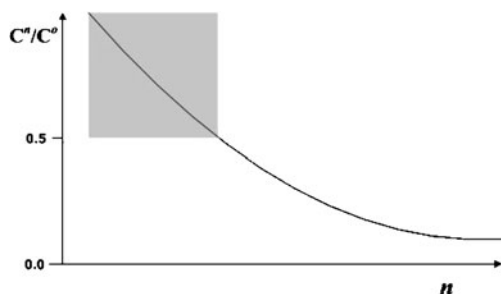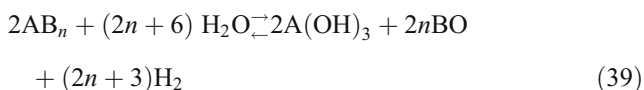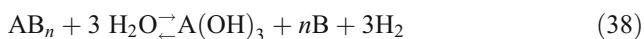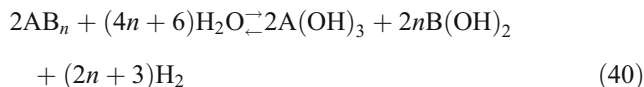$$+ (2n + 3)H_2 \qquad (39)$$

Fig. 3 Dependence discharge capacity change on number of charge–discharge cycles

$$2AB_n + (4n + 6)H_2O \underset{\leftarrow}{\rightarrow} 2A(OH)_3 + 2nB(OH)_2$$
$$+ (2n + 3)H_2 \qquad (40)$$

Disintegration of alloy during the work of MH electrode is caused by miscellaneous metal hydride formation on the electrode surface. Since these metal hydrides are characterized by different lattice volume expansion, some mechanic tensions appear at the grain boundaries and result in brittleness of hydrogen storage alloy/metal and increasing of local mobility for IMC metal atoms. In that case, the quantity of hydrogen-absorbing material decreases in proportion to the specific surface value. So the bigger is the alloy particle size, the less should be tendency of discharge capacity decay. In other words, the MH electrode stability depends on the size particle of hydrogen storage alloy/metal. Particle size decrease is accompanied by the disorder degree of metal matrix which finally may become amorphous.

Amorphous hydrogen storage alloys can also be used as effective MH electrodes. Discharge capacity values for amorphous alloys are not different from that for crystalline alloys [17]. Moreover, recently, studies of the MH electrode stability showed much better value for amorphous hydrogen storage alloys, strictly speaking by the absence of the mechanic tensions at charge–discharge cycling [18].

Hydrogen storage alloys for MH electrodes

There are many binary A_xB_y alloys which can be potential hydrogen storage materials for MH electrodes. These hydrogen storage alloys combine metal A whose hydrides generate heat exothermically with metal B whose hydride generates heat endothermically to produce the suitable binding energy so that hydrogen can be absorbed and desorbed at around room temperature and low pressure. Depending on how metals A and B are combined, their alloys are systematized in some big groups: AB_5 (the prototype alloy is $LaNi_5$); AB_2 (the prototype alloy is ZrV_2); and AB/A_2B (the prototype alloy is $TiNi/Ti_2Ni$). All of them should meet common requirements: the first is the hydrogen storage capacity achieved at ambient conditions; secondly, the oxidation and corrosion resistance in electrolyte is critical; thirdly, the reversibility of the hydrogenation process; and the last important thing is electrochemical kinetics.

MH electrodes based on AB_5 hydrogen storage alloys

The history of $LaNi_5$ as electrode material for Ni–MH accumulator begins from the 1970s [19, 20], but in practice, using that MH electrode had shown too high equilibrium

hydrogen pressure and too short cycle stability [21]. The loss of discharge capacity was attributed to the decomposition of $LaNi_5$ into $La(OH)_3$ and Ni. But pseudo-binary alloys where B metal was partly replaced by other transition metals helped change the thermodynamic properties [22–24]. The next point was improving cycle stability of $LaNi_5$ by partial substitution, $Ni \rightarrow Co$ [25]. Although these substitutions involved decreasing the hydrogen storage capacity, several compositions had been studied, and the best results were obtained from a mischmetal (Mm)-based three-substituted compound: $MmNi_{3.55}Mn_{0.4}Al_{0.3}Co_{0.75}$ [26, 27]. Use of mischmetal was only because of its lower price than lanthanum; moreover, $La \rightarrow Mm$ replacement gave better cycle stability [28].

In most cases, at partial A or B substitution for AB_5 alloys, crystal structure is not changed, but for every case, the limit of the substitution is individual. All these alloys crystallize in the $CaCu_5$-type structure ($P6/mmm$ space group) [29]. It is commonly observed that under hydrogenation, the structure is preserved too, but cell volume increases up to 25%. The stoichiometric $LaNi_5$ alloy shows desorption plateau pressure of 1.7 bar at room temperature which extends up to six H atom per formula unit (H/f.u.). Substitutions either on the nickel or on the lanthanum sublattices involve both a reduction of hydrogen storage capacity and change of equilibrium pressure. Some $La(Mm)Ni_{5-x}T_x$ alloys (where T = Al, Mn, Co) can be characterized by 0.01- to 1-bar plateau pressure that is very close to their requirements as MH electrodes [30–32].

The hydrogen storage capacity as well as theoretical discharge capacity of some prominent AB_5 alloys at ambient conditions (temperature and hydrogen pressure) [33] are presented in Table 1.

These examples of AB_5 alloys theoretically would show discharge capacity above 300 A·h/kg which is needed for effective electrode materials. In practice, during charge–discharge cycling, the values of discharge capacity gradually decreased because of huge cell volume expansion at hydrogenation. This large constraints lead to decrepitation of the grains, creating new fresh surfaces

Table 1 Hydrogen storage capacity and theoretical discharge capacity for some AB_5 alloys

Alloy	Hydrogen storage capacity (H/f.u.)	Temperature (K)	Hydrogen pressure (bar)	Theoretical discharge capacity (A·h/kg)
$LaNi_5$	6.24	313	25	387
$LaNi_{4.6}Mn_{0.4}$	6.21	313	10	386
$LaNi_{4.7}Al_{0.3}$	5.85	313	10	370
$LaNi_3Co_2$	5.39	313	10	334
$LaNi_4Cu$	5.45	313	10	334

susceptible to be corroded. What is more is that La mobility was increased toward such surfaces where it can be easily oxidized. Therefore, the effect of cell volume expansion on corrosion resistance under cycling was taken into account and proven by over-stoichiometrical alloys $La(Ni_{1-y}Cu_y)_{5+x}$ and $La(Ni_{1-y}Mn_y)_{5+x}$ which had a small lattice expansion [34–36].

The corrosion process of the AB_5 alloys leads to the formation of rare earth hydroxide which involves the formation of amorphous transition metal particles [37]. These corrosion products growing on a continuous nanocrystalline layer are composed of transition metals and metal oxides. Such surface modification is expected to be highly catalytic as regards to reverse electrochemical hydrogenation process. Therefore, some treatment like soaking in hot KOH solution or hydrogenytion–dehydrogenytion in hot air atmosphere had been tested to develop this catalytic layer at the grain surface. Kinetic improvements can be achieved by the addition of metal oxides as was shown in [38] with RuO_2 and Co_3O_4, which was attributed to increasing of electrocatalytic activity.

MH electrodes based on AB_2 hydrogen storage alloys

Laves phases are intermetallic compounds of AB_2 stoichiometry crystallizing among one of the three following structure types: $MgZn_2$ or $MgNi_2$ ($P6_3/mmc$ or C14) and $MgCu_2$ ($Fd3m$ or C15). They are one of the most represented groups in intermetallic compounds sharing this feature with $CaCu_5$-type compounds. The criterion for the existence of such phases in a metallic system A–B is mainly geometric: Atomic radius ratio R_A/R_B should be ~1.225. They belong to the topologically close-packed structure class and, as a consequence, are characterized by the unique presence of tetrahedral interstices and Fanck–Kasper coordination polyhedra [39].

In the sense of high-capacity Ni–MH accumulators, AB_2 Laves phases were considered as second-generation alloys after AB_5 alloys. But AB_2 alloys had much more difficulties: metallurgical problems related to the synthesis of single-phase compounds; adaptation of the equilibrium pressure to the application; and slow activation and high corrosion. These binary alloys are based on AB_2 intermetallic compounds with A = Zr, Ti and B = V, Cr, Mn. Except for TiV_2, all the binary compounds adopt either C14 or C15 structures or both. Some hydrogen absorption properties together with theoretical discharge capacity of these AB_2 alloys [40] are listed in Table 2.

Zr-based AB_2 alloys are characterized by a high stability and can absorb up to about 4 H/f.u. or even more as in the case of ZrV_2. Because of their mass, the theoretical discharge capacity is estimated as two times higher than for AB_5 alloys. On the other side, $TiCr_2$ possesses a

Table 2 Hydrogen storage capacity and theoretical discharge capacity for some AB_2 alloys

Alloy	Hydrogen storage capacity (H/f.u.)	Temperature (K)	Equilibrium hydrogen pressure (bar)	Theoretical discharge capacity (A·h/kg)
ZrV_2	5.4	323	$<10^{-8}$	750
$TiCr_{1.9}$	3.5	195	0.2	640
$ZrCr_2$	3.8	323	0.01	520
$ZrMn_2$	3.6	323	0.1	480
$TiMn_{1.6}$	2.0	293	12	390

moderate equilibrium pressure even at rather low temperatures [41, 42]. The case of $TiMn_2$ is peculiar due to its large binary compositional homogeneity domain, which allows a partial substitution of Mn by Ti to modify the stability of the hydride compound. As for the hydrides of AB_5 compounds, the general law predicting the linear increase of the plateau pressure as a function of the cell volume decreases is observed in many systems [43], which provides a valuable tool for selecting the right alloy composition with the convenient hydride stability. These modifications should be possible from a thermodynamic point of view, i.e., should lead to single-phase compounds with a Laves phase structure. For AB_2 alloys, A metal can be substituted mainly by Ti, which has a smaller atomic radius and less affinity for hydrogen; the B metal can be substituted either by other 3D transition metals (Fe, Co, Ni, and Cu) or even by Al. Owing to the reduced affinity for hydrogen and smaller atomic radii, such substitutions lead to a significant increase of the plateau pressure.

In a highly oxidizing electrolytic medium, AB_2 alloys behave dramatically worse than AB_5. They suffer from slow activation and low rate capabilities. Those drawbacks have been explained in terms of surface passivation due to the presence of a very dense layer formed by Zr and Ti oxides on the surface, blocking the electrochemical reaction [44] or increasing both hindrance to hydrogen diffusion and electrical resistance [45]. In order to overcome the main surface-related problems that disturb the electrochemical activity of AB_2 alloys, a lot of treatments have been tested: surface coating [46], hot charging treatment [47], and fluorination [48]. Surface coating allows protection from corrosion by covering the grains of the alloy with a thin non-oxidizable metal layer [49]. Hot charging treatment should dissolve the dense oxide layer at the surface of the grains in potassium hydroxide and leave Ni-rich layers on top of the surface to catalyze the charge transfer reaction [50]. Finally, fluorination techniques seem to improve the activation process by dissolving zirconium atoms and allowing precipitation of catalytic nickel [48].

MH electrodes based on AB/A_2B hydrogen storage alloys

In the early 1970s, the reversible hydrides of TiNi [51] and TiFe [52] were discovered. Due to their fast activation and low commercial price, they constitute the AB-type alloys with the most interesting hydrogenation properties, though their electrochemical applications were interrupted by the fast development of MH electrodes based on AB_5 alloys.

The most interesting AB hydrogen storage alloys are the Ti-based alloys TiFe, TiCo, and TiNi and the Zr-based alloys ZrNi and ZrCo. TiFe, TiCo, and ZrCo crystallize in the highly symmetrical CsCl-type cubic structure, whereas ZrNi has a CrB-type orthorhombic structure. The case of TiNi is particular since it presents a martensitic transformation around room temperature which is responsible for its remarkable shape memory behavior [53, 54]. The high-temperature phase, usually denoted as austenite, also exhibits a CsCl-type structure. On cooling, it transforms gradually into a monoclinic $P2_1/m$ structure, denoted as martensite, which has as prototype the TiNi alloy itself [55, 56].

Some hydrogen absorption properties together with theoretical discharge capacity of these AB alloys [57–59] are presented in Table 3.

Except for TiFe, all the hydrides formed by these AB alloys are characterized by high stability. Hydrogenation of TiFe by solid–gas reaction can only be achieved after severe activation treatments due to its high sensitivity to surface poisoning by gaseous impurities [60, 61]. However, partial substitutions of Fe by Mn and Ni are successful for improving the hydrogenation reactivity of the alloy and permit the adaptation of its plateau pressures for applications on hydrogen storage [62].

No invariant plateau region is observed for TiNi, which suggests a continuous solid solution of hydrogen in the parent alloy. Almost all studies on the hydrogenation properties of TiNi refer exclusively to austenite. However, martensite is expected to be present in TiNi-based alloys at room temperature or even above if selected partial substitutions are achieved. For example, in [63] have been

Table 3 Hydrogen storage capacity and theoretical discharge capacity for some AB alloys

Alloy	Hydrogen storage capacity (H/f.u.)	Temperature (K)	Equilibrium hydrogen pressure (bar)	Theoretical discharge capacity (A·h/kg)
TiFe	2.0	313	7−15	515
TiNi	1.4	403	0.2	355
TiCo	1.4	353	0.1	350
ZrCo	3.0	523	10^{-2}	535
ZrNi	2.8	473	10^{-1}–10^{-4}	500

shown that $Ti_{1-x}Zr_xNi$ alloys with $x<0.5$ can be produced either as martensite or as austenite when different quenching rates are used for the alloy preparation. Martensite presents a wide plateau pressure that expands in hydrogen concentration from 1 to 2.1 H/f.u.—two times higher than that of austenite. Thus, theoretical discharge capacity of martensitic Ti–Zr–Ni alloys would be about 550 A·h/kg.

Martensitic alloys suffer a severe pulverization upon hydrogenation, while austenitic ones are only embrittled. This behavior seems to be related to the precipitation of the hydride phase in martensite. It is worth mentioning that the martensitic transformation temperature may also be changed by hydrogenation processes [64]. The electrochemical properties of TiNi were first studied by Justi et al. [51] in two-phase Ti_2Ni–TiNi alloys. They found, by extrapolation of discharge capacities to single-phase TiNi electrodes, a reversible electrochemical capacity of 245 mAh/g for TiNi, i.e., corresponding to the desorption of 1 H/f.u. These electrodes degraded to 60% after 300 cycles. Gutjahr [65] confirmed the previous results in experiments with pure TiNi alloy and indicated that TiNi offers very good desorption kinetics and optimum surface conditions. In fact, it has been proven that the exchange current densities in this alloy are as high as in nickel Raney-type electrodes, and its electrocatalytic activity is very similar to that of $LaNi_5$ [66]. These properties could be related to the precipitation of metallic nickel clusters at the TiNi electrode surface upon electrolysis. Actually, transmission electron microscopy studies of the near-surface area of TiNi alloy revealed the formation of nickel precipitates after controlled gas oxidation [67]. Still concerning the kinetic properties of hydrogen in TiNi, it is worth mentioning that hydrogen absorption experiments at high temperatures (773–1,173 K) indicate that bulk hydrogen diffusion in TiNi is as fast as in TiFe [68].

If we have Ti_2Ni and TiNi in combination, TiNi demonstrate catalytic effect, and so they can influence the depth of electrochemical discharge. It means that under discharge, TiNiH can remain without changes because H atoms from $Ti_2NiH_{2.5}$ very easily fill up all possible vacancies of $TiNiH_{1-x}$. If there are no desorbed H atoms from $Ti_2NiH_{2.5}$ for TiNiH formation, the hydrogen quantity in TiNiH decreases to TiNi. Possible mechanism for phase transformation under charge–discharge cycling in Ti–Ni alloys should be the same as under hydrogen solid–gas reaction [69]:

$$TiNi + Ti_2Ni \overset{\rightarrow}{\leftarrow} TiNiH + Ti_2NiH_{0.5} \overset{\rightarrow}{\leftarrow} TiNiH + Ti_2NiH_{2.5} \qquad (41)$$
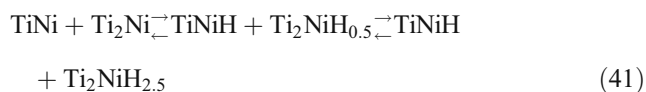
For example, $Ti_{3.87}Ni_{1.73}Fe_{0.7}O_{0.5}$ alloy consists of two hydrogen storage phases: $TiNi_{0.88}Fe_{0.28}$ and $Ti_{3.3}Fe_{0.7}Ni_2O_n$ ($n<0.5$) [70]. However, occupation of all possible vacations

in TiNi- and Ti_2Ni-type lattice by the most thermodynamically favorable H atoms took place simultaneously.

Ti_2Ni offers excellent fast discharge performance due to high diffusion of H atoms within its crystal lattice, but in spite of high charging capacity ($\sim$500 A·h/kg), its experimental discharge capacity is not more than 200 A·h/kg. In other words, the difference between charging and discharging capacities (irreversible capacity) is close to 300 A·h/kg [51]. In order to decrease irreversible capacity, for Ti_2Ni alloys, oxygen modification has been done [71–77]. Therefore, experimentally, 360 A·h/kg for $Ti_{3.87}Ni_{1.73}Fe_{0.7}O_{0.2}$ alloy was traced, that corresponding to high reversible hydrogen storage capacity ($\sim$6.5H/f.u.) [77].

Unfortunately, the cycle life of biphasic Ti–Ni electrodes is poor because of corrosion and oxidation of the Ti_2Ni phase [51]. This effect is probably accelerated by the pulverization of this phase due to the discrete lattice expansion accompanying the formation of Ti_2Ni hydrides, as occurs in AB_5-type alloys [34]. Wakao et al. [78] have reported that the cycle stability and discharge capacity of Ti–Ni electrodes are improved by partial substitutions of Ti by Zr. For instance, $Ti_{0.8}Zr_{0.2}Ni_{0.6}$ electrodes present a discharge capacity of 370 A·h/kg. This behavior was tentatively attributed to the formation of a more stable passive film which protects the underlying electrode from oxidation. Unfortunately, the properties of such electrodes were strongly dependent on their preparation procedure, and no metallurgical characterization of the alloys was given.

Conclusions

About 30 years ago, the first experiments on MH electrodes were carried out, and so far, mostly for AB_5 alloys, their application in Ni–MH accumulators has been done. Research on AB_2 and AB/A_2B alloys, which possess much more complicated metallurgical aspects, is in permanent progress. There is confidence to achieve in the next future MH electrodes based on these hydrogen storage alloys with all general requirements.

From this review, one can conclude that high hydrogen storage capacity can be achieved by many binary or multicomponent alloys; consequently, theoretical discharge capacity would be suitable for high-capacity electrode. But in practice, it is not so easy to reach more than 50% of maximal possibility. From a thermodynamical point of view, the range of enthalpy of metal hydride formation (ΔH) should be from -25 to -50 kJ/mol, which would be suitable for hydrogen storage alloys as MH electrodes [79, 80]. In this case, electrode material would be reversible with respect to hydrogenation process.

The next important thing is electrochemical kinetics. Determination of the limiting stage would give a clearer

picture of multi-stage electrochemical hydrogenation and, consequently, the possibility to evaluate velocity of hydrogenation. Hydrogen diffusion in the bulk of hydrogen storage alloy (mass transfer process) should be the rate-determining reaction, while the velocity of charge transfer reaction at the MH electrode surface is very high [81]. This means that the high-rate charge–discharge capability of the Ni–MH accumulators can be limited by the hydrogen diffusion reaction in the hydrogen storage alloy.

Mostly because of charge–discharge cycling in oxidizing electrolyte, different types of corrosion are present under MH electrode performance. Thus, cycle stability will depend on surface properties and working regime of the electrodes. The main disadvantage of conventional Ni–MH accumulators today is low capacity retention characteristic. This problem involved not only chemical stability of all components in alkaline water solution but also physical and mechanical reliability of manufacturing MH electrode. Two technical approaches are possible to attain this characteristic: short charging time or reducing self-discharge [82]. The sharp drop in Ni–MH accumulator charging efficiency at high temperature is due to the decline in oxygen overpotential of the nickel electrode, and it is known that adding oxides of heavy rare earths such as Er, Tm, Yb, or Lu effectively prevents this. It is also effective for charge acceptance when charging with a large current, making capability of at least 90% possible even in a 15-min charge. Self-discharge can be minimized through inhibition of reduction reaction of NiOOH by hydrogen or water to $Ni(OH)_2$ and decreasing shuttle reactions of impurity ions from the separator and both positive and negative electrodes.

Taking into account values of discharge capacity, high rate discharge, and possibility of fast charging for MH electrodes, it makes sense still to develop studies on Ni–MH accumulators which are expected to show much better characteristics than their precursors.

References

1. Ovsinsky SR, Fetcenko MA, Ross J (1993) Science 260:176–181
2. Mariaka Y, Nakuwara S, Itou T (2001) J Power Sources 100:107–116
3. Soria ML, Chacón J, Hernándes JC (2001) J Power Sources 102:97–104
4. Takamura T (2002) Solid State Ionics 152–153:19–34
5. Sakai T, Matsuoka M, Iwakura C (1995) Rare-earth intermetallics for metal-hydrogen batteries. Elsevier Science, Berlin
6. Semenenko KN (1979) Hydrogen—the base of chemical technology and energy of a future. Znanie, Moscow
7. Wójcik G, Kopczyk M, Drulis H, Bełtowska-Brzezińska M (1995) Wiad Chem 49:5–6
8. Kleperis J, Wójcik G, Czerwinski A, Skowronski J, Kopczyk M, Bełtowska-Brzezińska M (2001) J Solid State Electrochem 5:229–249
9. Ledovskikh A, Verbitsky E, Ayeb A, Notten PHL (2003) J Alloys Comp 356–357:742–745
10. Iwakura C, Asaoka T, Yoneyyama H, Sakai T, Ishikawa H, Oguro K (1988) Nippon Kagaku Kaishi 8:1482–1488
11. Zhu W-H, Zhang D-J, Ke J-J (1996) Mater Research Bull 31:73–682
12. Krstajic NV, Grgur BN, Zdujic M, Vojnovic MV, Jakšić MM (1997) J Alloys Comp 257:245–252
13. Jakšić MM (1995) Electrochem Acta 29:1539–1550
14. Saldan I, Frenzel J, Shekhah O, Chelmowski R, Birkner A, Wöll Ch (2009) J Alloys Comp 470:568–573
15. Petrii OA, Vasina SYa, Korobov II (1996) Achievements of Chemistry 65:195–208
16. Solonin YuM, Kolomiets LL, Skhorohod VV (1993) Hydrogen-absorbing alloys for Ni–MH power sources. IPM-NASU, Kyiv
17. Ryan DH, Dumais F, Patel B (1991) J Less-Common Met 172–174:1246–1251
18. Zhang S-L, Zhao Y-T, Chen G, Cheng X-N, Sun H-Q (2008) J Mater Process Technol 198:270–274
19. Bronoël G, Sarradin J, Bonnemay M, Percheron-Guégan A, Achard JC, Schlapbach L (1976) Int J Hydrogen Energy 1:251
20. Percheron-Guégan A, Achard JC, Sarradin J, Bronoël G (1978) Hydrides for energy storage. Pergamon, Oxford
21. Bittner HF, Badcock CC (1983) J Electrochem Soc 130:193
22. Van Mal HH, Buschow KHJ, Miedema AR (1974) J Less-Common Met 35:65
23. Diaz H, Percheron-Guégan A, Achard JC, Chatillon C, Mathieu JC (1979) Int J Hydrogen Energy 4:445
24. Lartigue C, Percheron-Guégan A, Achard JC, Tasset F (1980) J Less-Common Met 75:23
25. Willems JJG (1984) Philips J Res Suppl 39:1
26. Ikoma M, Kawano H, Matsumoto I, Yanagihara N (1987) Eur Patent application no. 271043
27. Ogawa H, Ikoma M, Kawano H, Matsumoto I (1988) J Power Sources 12:393
28. Adzic GD, Johnson JR, Reilly JJ, McBreen J, Mukerjee S (1995) J Electrochem Soc 142:3429
29. Percheron-Guégan A, Lartigue C, Achard JC (1985) J Less-Common Met 109:287
30. Achard JC, Percheron-Guégan A, Diaz H, Briaucourt F, Demany F (1977) In: Hydrogen in metals. 2nd International Congress, Paris
31. Colinet C, Pasturel A, Percheron-Guégan A, Achard JC (1987) J Less-Common Met 134:109
32. Van Mal HH, Buschow KHJ, Kuijpers FA (1973) J Less-Common Met 32:289
33. Cuevas F, Joubert JM, Latroche M, Percheron-Guégan A (2001) Appl Phys A 72:225–238
34. Notten PHL, Einerhand REF, Daams JLC (1994) J Alloys Compd 210:221
35. Notten PHL, Daams JLC, Einerhand REF (1994) J Alloys Compd 210:233
36. Notten PHL, Latroche M, Percheron-Guégan A (1999) J Electrochem Soc 146:3181
37. Maurel F, Knosp B, Backhaus-Ricoult M (2000) J Electrochem Soc 147:78
38. Iwakura C, Fukumoto Y, Matsuoka M, Kohno T, Shinmou K (1993) J Alloys Compd 192:152
39. Sinha AK (1972) Prog Mater Sci 15:79
40. Buschow KHJ, Bouten PCP, Miedema AR (1982) Rep Prog Phys 4:937
41. Johnson JR, Reilly JJ (1978) Inorg Chem 17:3103
42. Johnson JR (1980) J Less-Common Met 73:345
43. Fujitani S, Yonezu I, Furukawa N, Akiba E, Hayakawa H, Ono S (1991) J Less-Common Met 172–174:220
44. Liu FJ, Ota H, Okamoto S, Suda S (1997) J Alloys Compd 253–254:452

45. Lee HH, Lee KY, Lee JY (1997) J Alloys Compd 253–254:601
46. Iwakura C (1985) Denki Kagaku 53:722
47. Kim DM, Liang KJ, Lee JY (1999) J Alloys Compd 293–295:583
48. Liu BH, Li ZP, Higuchi E, Suda S (1999) J Alloys Compd 293–295:702
49. Blair S (2000) Canadienne sur l'Hydrog'ene, Proceedings of the 10th Conference, Quebec, Canada
50. Liu BH, Lee JY (1997) J Alloys Compd 255:43
51. Justi EW, Ewe HH, Kalberlah AW, Saridakis NM, Schaefer MH (1970) Energy Convers 10:183
52. Reilly JJ, Wiswall RH (1974) Inorg Chem 13:218
53. Otsuka K, Ren X (1999) Intermetallics 7:511
54. Otsuka K, Ren X (1999) Mater Sci Eng A 273–275:89
55. Fruchart D, Soubeyroux JL, Miraglia S, Obbade S, Lorthioir G, Basile F, Colin D, Faudot F, Ochin P, Dezellus A (1993) Z Phys Chem 179:225
56. Kudoh Y, Tokonami M, Miyazaki S, Otsuka K (1985) Acta Metall 33:2049
57. Burch R, Mason NB (1979) J Chem Soc Faraday Trans I 75:561
58. Irvine SJC, Harris IR (1980) J Less-Common Met 74:33
59. Luo W, Craft A, Kuji T, Chung HS, Flanagan TB (1990) J Less-Common Met 162:251
60. Sandrock GD, Goodell PD (1984) J Less-Common Met 104:159
61. Schlapbach L (1992) In: Schlapbach L (ed) Hydrogen in intermetallic compounds II. Springer, Berlin
62. Sandrock GD (1999) J Alloys Compd 293–295:877
63. Cuevas F, Latroche M, Ochin P, Dezellus A, Fernández JF, Sánchez C, Percheron-Guégan A (2000) Metal–hydrogen systems—fundamentals and applications. Proceedings of International Symposium Noosa, Australia
64. Damiani C, Pelegrina JL, Ahlers M (1999) J Alloys Compd 284:243
65. Gutjahr MA (1974) PhD thesis, Geneva University
66. Machida K, Enyo M, Adachi G, Shiokawa J (1984) Electrochim Acta 29:807
67. Venkert A, Dariel MP, Talianker M (1984) J Less-Common Met 103:361
68. Schmidt R, Schlereth M, Wipf H, Assmus W, Müllner M (1989) J Phys I 1:2473
69. Buchner H, Gutjahr MA, Beccu KD, Säufferer H (1972) Z Metallk 63:497–500
70. Saldan I, Frenzel J, Shekhah O, Chelmowski R, Birkner A, Wöll Ch (2009) J Alloys and Comp 470:568–573
71. Zavaliy I, Wojcik G, Mlynarek G, Saldan I, Yartys V, Kopczyk M (2001) J Alloys and Comp 314:124–131
72. Takeshita HT, Tanaka H, Kiyobayashi T, Takeichi N, Kuriyama N (2002) J Alloys and Comp 330–332:517–521
73. Zavaliy I, Saldan I (2002) Mater Sci 38:53–60
74. Saldan I, Koval'chuk I, Zavaliy I (2003) Mater Sci 39:70–76
75. Saldan IV (2004) PhD thesis, Lviv University
76. Saldan I, Dubov Y, Riabov A, Zavaliy I (2006) Mater Sci 42:56–64
77. Saldan I, Burtovyy R, Becker HW, Ader V, Wöll Ch (2008) J Hydrogen Energy 33:7177–7184
78. Wakao S, Yonemura Y, Nakano H, Shimada H (1984) J Less-Common Met 104:365
79. Hong K (2001) J Power Sources 96:85–89
80. Ovshinsky SR, Fetchenko MA (2001) Appl Phys A Mater Sci Process 72:239–244
81. Geng M, Northwood DO (2003) J Hydrogen Energy 28:633–636
82. Watada M, Kuzuhara M, Oshitani M (2006) GS Yuasa Tech Report 12:46–53